

Received April 27, 2021, accepted May 27, 2021, date of publication June 2, 2021, date of current version June 9, 2021.

Digital Object Identifier 10.1109/ACCESS.2021.3085304

# Three-Dimensional Ultra-Short Base Line Based Underwater Acoustical Localization Utilizing Modified Newton Algorithm

XIANG LI<sup>1</sup>, XIN LIU<sup>2</sup>, LONG QU<sup>3</sup>, YI LOU<sup>4</sup>, AND SIBO SUN<sup>4</sup>

<sup>1</sup>Acoustic Science and Technology Laboratory, Harbin Engineering University, Harbin 150001, China

<sup>2</sup>Key Laboratory of Marine Information Acquisition and Security (Harbin Engineering University), Ministry of Industry and Information Technology, Harbin 150001, China

<sup>3</sup>703 Research Institute, China State Shipbuilding Corporation Ltd., Harbin 150001, China

<sup>4</sup>College of Underwater Acoustic Engineering, Harbin Engineering University, Harbin 150001, China

Corresponding author: Yi Lou (louyi@hrbeu.edu.cn)

**ABSTRACT** The ultra-short base line (USBL) is a widely used technique in achieving the underwater acoustic localization (UWAL). Aimed at increasing the localization precision, we propose a three-dimensional (3-D) USBL based UWAL method utilizing the modified Newton algorithm. Firstly, a modified Newton algorithm is proposed by introducing the singular value factor to address the non-convergence problem, which dramatically deteriorate the localization precision in the traditional Newton algorithm. Secondly, a localization node selection algorithm is presented to optimize the localization precision and reduce the computational burden. Moreover, the localization precision analysis is implemented to evaluate the theoretical performance of the method. Finally, simulation and lake trial results prove the effectiveness of the method.


**INDEX TERMS** Underwater acoustic localization (UWAL), ultra short base line (USBL), direction of arrival (DOA), Newton algorithm.

## I. INTRODUCTION

Underwater localization is widely used in underwater active/passive detection, autonomous underwater vehicle docking, underwater monitoring, and plays an important role in sea exploration. The existing underwater localization system mainly includes the underwater acoustic localization (UWAL) system and the underwater optical/wireless localization networks [1]–[4]. Since the propagation loss of the acoustic signal is much lower than that of the optic signal or the wireless signal in the water, the UWAL is the most effective way to achieve the long-range underwater localization [5]–[8].

According to the information used, most of the UWAL methods can be divided into two categories, that is the long baseline (LBL) localization method and the ultra-short base line (USBL) localization method. The LBL localization method measures the time of arrival (TOA) of the acoustic signal, calculates the range information between the

localization nodes and the target, and solves the target's coordinate based on the range information. In the last decade, many methods have been proposed for the LBL based UWAL, addressing the practical problems in real scene. Stratification effect is a severe problem in deep sea, Zhang *et al.* [9] employ the Gauss-Newton algorithm based UWAL method to solve the problem and achieves a joint estimation of the time synchronization and localization. Jamalabdollahi and Zekavat [10] propose an effective ranging approach considering the nonhomogeneous media consisting of frequency dispersive sub-media. Li *et al.* [11] apply a Bayesian inference algorithm to compensate the underwater vehicle's motion during the interrogation-reception time interval. Thomson *et al.* [12] present a linearized Bayesian inversion algorithm, which has a high robustness against node's position measurement noise and sound speed measurement noise. Utilizing the single-input-multiple-output (SIMO) model, Sun [13] achieves the simultaneous UWAL of a group autonomous underwater vehicle (AUV) based on single beacon, and develops the second-order time different of arrival algorithm to compensate the drifted signal period of the black

The associate editor coordinating the review of this manuscript and approving it for publication was Haiquan Zhao .

box [14], [15], which can be applied in searching the sunken airplane.

On the other hand, the USBL based UWAL methods estimate the direction of arrival (DOA) information utilizing a sensors' array and solve the target's position utilizing the DOA information obtained from several localization nodes. The recent improvement of the USBL based UWAL methods concentrates on increasing the DOA estimation accuracy to improve the localization precision. Ma *et al.* [16] and Zheng *et al.* [17] propose a Bayesian learning algorithm, which increase the DOA measurement precision in impulsive noise environments. Varanasi *et al.* [18] address the near field DOA estimation via introducing the signal invariant and direction independent spherical harmonic features. Hefner and Dzikowicz develop a spiral wave front beacon, which has a high robustness in multipath environments where reflected or channeled rays are present [19], [20]. Combing the coherent signal subspace processing and compressed sensing theory, Li *et al.* achieve the DOA estimation for wideband weak targets [21] and quantify the pseudo-peaks in the DOA estimation and gives a detection threshold selection algorithm to improve the estimation precision [22]. Compared with the LBL based UWAL methods, the USBL based UWAL methods need a more complex hardware and software design but bring two advantages. 1) The methods do not rely on the pulse signal, and hence can achieve the passive moving target detection utilizing the sailing noise. 2) The methods do not need the sound speed information and have a high robustness in different sea environments.

This paper focuses on increasing the localization precision for the USBL based UWAL method. Firstly, the Newton algorithm is utilized to solve the non-linear optimization problem in the conventional USBL based UWAL method. However, when the initial value is improper in real scene, the Newton algorithm suffers from a low convergence probability especially for the 3-dimensional (3-D) case [23], which dramatically deteriorates the localization precision. To improve the convergence probability, we propose a modified Newton algorithm, which introduces the singular value factor to cure the ill-condition partial derivative matrix. Secondly, the localization precision is closely related to the position of the localization nodes. The localization node placement is an effective way to further improve the localization precision. On this point, a localization node selection algorithm is presented, which optimizes the localization precision and reduces the computational burden. Besides, the localization precision analysis evaluates the theoretically performance of the proposed method and the lake trial validates the effectiveness of the proposed method.

The rest of this paper is organized as follows: In Section II, the geometrical configuration for the 3-D USBL model is presented. In Section III, the equation set to solve the target's coordinate is established and the localization precision of the equation set is analyzed. In Section IV, the modified Newton algorithm is proposed to solve the equation set. In Section V, the localization node selection algorithm is presented. The

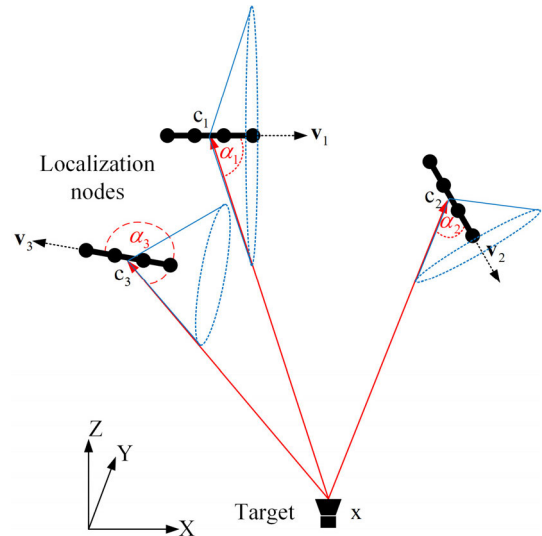


FIGURE 1. Geometrical configuration for the 3-D USBL.

simulation and the lake trial are implemented in Section VI and Section VII concludes our work.

## II. GEOMETRICAL CONFIGURATION FOR THE 3-D USBL

A typical geometrical configuration for the 3-D USBL based UWAL problem is given in Figure 1, where, a global coordinate system is established. X axis indicates the East direction, Y axis indicates the North direction, and Z axis indicates the vertical up. The target transmits periodic acoustical signals, whose coordinate is denoted as  $\mathbf{x} = [x, y, z]$  in the given coordinate system. The localization nodes receive the acoustic signal using an array of microphone, and measure the DOA of the signal as  $\alpha_n$ , where,  $n \in [1, 2, \dots, N]$  is the tag of the node. The coordinates of the nodes and the direction of the microphone array are denoted as  $\mathbf{c}_n = [a_n, b_n, c_n]$  and  $\mathbf{v}_n = [u_n, v_n, w_n]$ , respectively. We should notice that different localization nodes can be different receives at one time or a moving receiver at different time.

Since the DOA indicates the angle between the direction of the microphone array and the line of sight (LOS) of the target, it can be expressed as:

$$\cos \alpha_n = \frac{(\mathbf{c}_n - \mathbf{x}) \cdot \mathbf{v}_n}{\|\mathbf{c}_n - \mathbf{x}\|_2 \|\mathbf{v}_n\|_2} \quad (1)$$

where,  $\|\cdot\|_2$  indicates the modulus of the vector. (1) establishes the relationship between the angular measurement  $\alpha_n$  and the unknow target's coordinate  $\mathbf{x}$ . The USBL based UWAL methods utilize the angular information to solve the coordinate of the target.

## III. LOCALIZATION METHOD FOR THE 3-D USBL

### A. LOCALIZATION METHOD

From (1), each localization node indicates a cone with  $\mathbf{c}_n$  as the apex and  $2\alpha_n$  as the cone-apex angle. Combine the angular information from different nodes, the equation set of

the localization problem is established as:

$$\begin{cases} f_1(\mathbf{x}) = \arccos \frac{(\mathbf{c}_1 - \mathbf{x}) \cdot \mathbf{v}_1}{\|\mathbf{c}_1 - \mathbf{x}\|_2 \|\mathbf{v}_1\|_2} - \alpha_1 = n_1 \\ f_2(\mathbf{x}) = \arccos \frac{(\mathbf{c}_2 - \mathbf{x}) \cdot \mathbf{v}_2}{\|\mathbf{c}_2 - \mathbf{x}\|_2 \|\mathbf{v}_2\|_2} - \alpha_2 = n_2 \\ \vdots \\ f_N(\mathbf{x}) = \arccos \frac{(\mathbf{c}_N - \mathbf{x}) \cdot \mathbf{v}_N}{\|\mathbf{c}_N - \mathbf{x}\|_2 \|\mathbf{v}_N\|_2} - \alpha_N = n_N \end{cases} \quad (2)$$

where,  $n_1, n_2, \dots, n_N$  are the measurement noise of the target's angle (affected by the signal-to-noise ratio, the shape of the array, the array signal processing algorithm, and the sound bend effect [24]).

To solve the three unknowns ( $[x, y, z]$ ) of the target's coordinate, at least three equations (nodes) are needed. In this case, the localization problem is essentially a cone intersection problem. The target locates at the intersection of the three cones determined by the three equations as shown in Figure 1. If the number of the nodes is more than three, the problem is converted to an optimization problem. The solution of  $\mathbf{x}$  is with the minimum value of cost function:

$$\mathbf{x} = \arg \min \mathbf{f}(\mathbf{x})^T \mathbf{Q}_n^{-1} \mathbf{f}(\mathbf{x}) \quad (3)$$

where,  $\mathbf{f} = [f_1 \ f_2 \ \dots \ f_N]$ ,

$$\mathbf{Q}_n = E([n_1, n_2, \dots, n_N]^T [n_1, n_2, \dots, n_N]).$$

Since (2) is a non-linear equation set, it is hard to give the analytical solution. The numerical analysis algorithms should be applied to calculate the numerical solution. The Newton algorithm is the most widely used numerical analysis algorithm owing to its low computational burden and high convergence speed. However, since the Newton algorithm is the linear approximation of an infinitesimal element, the algorithm suffers from a low convergence probability if an improper initial value is installed. Especially for the 3-D USBL based UWAL, the high order non-linear equation set enlarges the influence of the improper initial value, which dramatically decline the localization precision. In this case, a modified Newton algorithm is presented in the next section to address the problem, but before that, the localization precision is analyzed as the following content to show the theoretical performance of the proposed 3-D USBL based UWAL model.

### B. LOCALIZATION PRECISION ANALYSIS

In this sub-section, we introduce horizontal dilution of precision (HDOP) as the criteria to evaluate the localization precision. The HDOP of the 3-D USBL based UWAL model is given as:

$$\mathbf{D}_x = \mathbf{M}_x^{-1} \cdot (\mathbf{M}_\alpha \cdot \mathbf{D}_\alpha \cdot \mathbf{M}_\alpha^T + \mathbf{M}_{c1} \cdot \mathbf{D}_{c1} \cdot \mathbf{M}_{c1}^T + \mathbf{M}_{c2} \cdot \mathbf{D}_{c2} \cdot \mathbf{M}_{c2}^T + \dots + \mathbf{M}_{cN} \cdot \mathbf{D}_{cN} \cdot \mathbf{M}_{cN}^T) \cdot \mathbf{M}_x^{-1T} \quad (4)$$

$$\text{HDOP} = \text{trace}(\mathbf{D}_x) \quad (5)$$

TABLE 1. Geometrical parameters and noise environment.

Node's coordinate	Node's coordinate	Node's coordinate
$\mathbf{c}_1$	$\mathbf{c}_2$	$\mathbf{c}_3$
[0 300 0] m	[260 -150 0] m	[-260 -150 0] m
Node's velocity	Node's velocity	Node's velocity
$\mathbf{v}_1$	$\mathbf{v}_2$	$\mathbf{v}_3$
[5 0 0] m/s	[-2.5 -4.3 0] m/s	[2.5 -4.3 0] m/s
Target's coordinate	RMSE of the DOA information	RMSE of the node's coordinate
[100 50 -300] m	0.5 degree	1.8 m

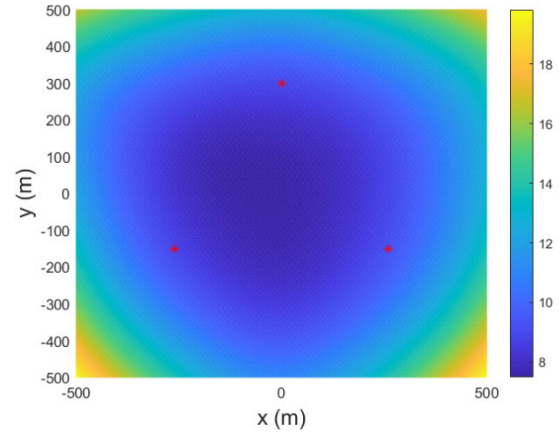


FIGURE 2. Distribution of the localization precision.

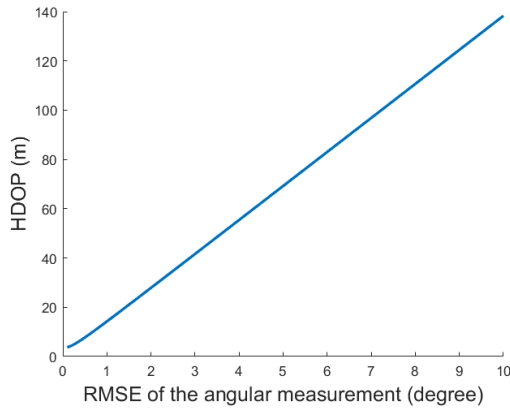
where,  $\text{trace}(\ast)$  indicates the trace of the matrix.  $\mathbf{D}_x \ \mathbf{D}_\alpha \ \mathbf{D}_{cN}$  are the covariance matrices for the target's coordinate error, the angular measurement error, the node's coordinate measurement error, respectively. The angular measurement error and the node's coordinate measurement error are supposed to be independent, 0-mean, and Gauss distributed.  $\mathbf{M}_x \ \mathbf{M}_\alpha \ \mathbf{M}_{cN}$  are the corresponding partial derivative matrices. Detailed expressions of these matrices are given in the Appendix.

Utilizing (4) and (5), the distribution of the localization precision related to different target's positions is shown in Figure 2, where, the red asterisk marks the position of the localization nodes. The geometrical parameters and the noise environment are listed in Table 1.

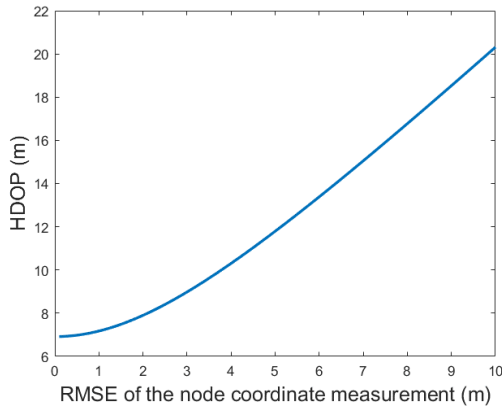
From Figure 2, for the shown 1 km<sup>2</sup> area, the HDOP is lower than 20 m, and the mean HDOP of the area is 12.6 m. For the triangular area surrounded by the localization nodes (red asterisk), the HDOP is lower than 10 m, and the mean HDOP is 8.9 m. Figure 2 reveals a high localization precision of the model, which is influenced by the noise environment.

From Figure 2, for the shown 1 km<sup>2</sup> area, the HDOP is lower than 20 m, and the mean HDOP of the area is 12.6 m. For the triangular area surrounded by the localization nodes (red asterisk), the HDOP is lower than 10 m, and the mean HDOP is 8.9 m. Figure 2 reveals a high localization precision of the model, which is influenced by the noise environment.

Next, we test the robustness of the model against measurement noises. The tested measurement noise includes the



(a) Distribution of the localization precision.



(b) Node's coordinate noise

FIGURE 3. Robustness test against measurement noises.

angular measurement noise (usually affected by the aperture of the sensor's array and the signal-to-noise ratio) and the node's coordinate measurement noise (from global coordinate system error or the inner navigation system error). When we test either noise, the other noise is set to be a constant as Table 1. Without losing the generalization, the coordinate of the target is fixed at [100 50 -300] m. The result of the robustness test is shown in Figure 3.

From Figure 3, the HDOP varies rapidly with the RMSE of the DOA, which indicates that the model has a low robustness against the angular measurement noise. While the HDOP varies slowly with the RMSE of the node's coordinate, and the model has a high robustness against the node's coordinate measurement noise. For most real scene, the DOA measurement noise is lower than 1 degree and the node's coordinate measurement noise is lower than 5 m. In this case, the corresponding localization precision is higher than 20 m.

Localization precision analysis indicates that the proposed 3-D USBL based UWAL model ensures a high localization precision if the equation set is correctly solved. However, in real situation, the incorrect initial value may lead to a nonconvergence solution of the equation set. In this case, the localization performance is dramatically deteriorated.

#### IV. SOLVING OF THE EQUATION SET UTILIZING THE MODIFIED NEWTON ALGORITHM

##### A. TRADITIONAL NEWTON ALGORITHM

The traditional Newton algorithm is derived from Taylor decomposition as:

$$\mathbf{F}(\mathbf{x}) = \mathbf{F}(\mathbf{x}_0) + \mathbf{F}'(\mathbf{x}_0)(\mathbf{x} - \mathbf{x}_0) + \frac{\mathbf{F}''(\mathbf{x}_0)(\mathbf{x} - \mathbf{x}_0)^2}{2!} + \dots + \frac{\mathbf{F}^{(n)}(\mathbf{x}_0)(\mathbf{x} - \mathbf{x}_0)^n}{n!} + \dots \quad (6)$$

where,  $\mathbf{x}_0$  is the initial value of  $\mathbf{x}$ . Neglecting the higher order terms ( $\geq 2$ ) and substituting (2) into (6), we have:

$$\mathbf{F}(\mathbf{x}_0) + \mathbf{F}'(\mathbf{x}_0)(\mathbf{x} - \mathbf{x}_0) = 0 \quad (7)$$

Then, the traditional Newton iterative equations are given by:

$$\mathbf{x}_{m+1} = \mathbf{x}_m + \Delta \mathbf{x}_m \quad (8)$$

$$\Delta \mathbf{x}_m = [\mathbf{f}'(\mathbf{x}_m)]^{-1} \cdot \mathbf{f}(\mathbf{x}_m) \quad (9)$$

where,  $\mathbf{x}_m$  is the state vector in each iteration and  $m \in [1 \ 2 \ \dots \ M]$  is the step of the iteration the equation can be derived, as shown at the bottom of next page.

To calculate the inverse of the matrix  $\mathbf{f}'(\mathbf{x}_m)$ , singular value decomposition is implemented, and  $\mathbf{f}'(\mathbf{x}_m)$  can be expressed as:

$$\mathbf{f}'(\mathbf{x}_m) = \mathbf{U}\mathbf{\Omega}\mathbf{V} = \sum_{i=1}^N \sigma_i \mathbf{u}_i \mathbf{v}_i^T \quad (10)$$

$$\mathbf{U} = [\mathbf{u}_1 \ \mathbf{u}_2 \ \dots \ \mathbf{u}_N] \quad (11)$$

$$\mathbf{V} = [\mathbf{v}_1 \ \mathbf{v}_2 \ \dots \ \mathbf{v}_N] \quad (12)$$

$$\mathbf{\Omega} = \text{diag}(\sigma_1 \ \sigma_2 \ \dots \ \sigma_N) \quad (13)$$

where,  $\mathbf{U}$  and  $\mathbf{V}$  are the triangular matrixes.  $\mathbf{\Omega}$  is the diagonal matrix.  $\sigma_n$  is the singular value of the matrix  $\mathbf{f}'(\mathbf{x}_m)$ .  $\mathbf{u}_n$  and  $\mathbf{v}_n$  are the corresponding left and right singular vectors, respectively. Utilizing the singular value decomposition, the iterative equation of the traditional Newton algorithm is given as:

$$\Delta \mathbf{x}_m = \sum_{i=1}^N \frac{\mathbf{u}_i \mathbf{f}(\mathbf{x}_m) \mathbf{v}_i}{\sigma_i} \quad (14)$$

From (9) and (14), the  $\Delta \mathbf{x}_m$  is with the minimum  $\|\mathbf{f}'(\mathbf{x}_m)\Delta \mathbf{x}_m - \mathbf{f}(\mathbf{x}_m)\|_2^2$  as:

$$\Delta \mathbf{x}_m = \arg \min \|\mathbf{f}'(\mathbf{x}_m)\Delta \mathbf{x}_m - \mathbf{f}(\mathbf{x}_m)\|_2^2 \quad (15)$$

The traditional Newton algorithm is widely applied in solving the lower order non-linear problem. However, when the algorithm is applied to the 3-D USBL based UWAL model. Due to the following problems:

- 1) The equation set (2) is a high order non-linear problem,
- 2) The initial value  $\mathbf{x}_0$  is far from its real value  $\mathbf{x}$ ,
- 3) The input errors ( $\mathbf{D}_\alpha \ \mathbf{D}_{cn}$ ) disturbs the solution form (4), the matrix  $\mathbf{f}'(\mathbf{x}_m)$  has the potential to be an ill-conditioned matrix with the magnitudes of the singular value distributing in a large range. In this case,



$\|\mathbf{f}'(\mathbf{x}_m)\Delta\mathbf{x}_m - \mathbf{f}(\mathbf{x}_m)\|_2^2$  is insensitive with  $\Delta\mathbf{x}_m$  from (15), and a large magnitude of  $\Delta\mathbf{x}_m$  is calculated from (14), which leads to a nonconvergence iteration.

### B. MODIFIED NEWTON ALGORITHM

To solve the nonconvergence problem, a modified Newton algorithm is proposed in this sub-section. Introducing the Tikhonov technique, a modified equation of (15) is established as:

$$\Delta\mathbf{x}_m = \arg \min(\|\mathbf{f}'(\mathbf{x}_m)\Delta\mathbf{x}_m - \mathbf{f}(\mathbf{x}_m)\|_2^2 + \lambda^2 \|\Delta\mathbf{x}_m\|_2^2) \quad (16)$$

Based on (16), the corresponding iterative equation is given as:

$$\Delta\mathbf{x}_m = \sum_{i=1}^N \frac{\sigma_i^2}{\sigma_i^2 + \lambda^2} \frac{\mathbf{u}_i \mathbf{f}'(\mathbf{x}_m) \mathbf{v}_i}{\sigma_i} \quad (17)$$

where,  $\lambda$  is the singular value factor and  $t_i = \frac{\sigma_i^2}{\sigma_i^2 + \lambda^2}$  means the filter factor.

In (16) and (17), we should notice the following facts.

1) Introducing the filter factor, the sensitivity of  $\|\mathbf{f}'(\mathbf{x}_m)\Delta\mathbf{x}_m - \mathbf{f}(\mathbf{x}_m)\|_2^2$  related to  $\Delta\mathbf{x}_m$  is increased. While  $\mathbf{f}'(\mathbf{x}_m)$  is an ill-conditioned matrix,  $\Delta\mathbf{x}_m$  mainly variates with the second term ( $\lambda^2 \|\Delta\mathbf{x}_m\|_2^2$ ), which avoids the large magnitude of  $\Delta\mathbf{x}_m$ . While  $\mathbf{f}'(\mathbf{x}_m)$  is a normal matrix,  $\Delta\mathbf{x}_m$  mainly variates with the first term ( $\|\mathbf{f}'(\mathbf{x}_m)\Delta\mathbf{x}_m - \mathbf{f}(\mathbf{x}_m)\|_2^2$ ), and the convergence is guaranteed.

2) In the modified Newton algorithm, the singular value becomes  $(\sigma_i^2 + \lambda^2)/\sigma_i$ . Therefore, the condition of the matrix  $\mathbf{f}'(\mathbf{x}_m)$  is modified to be  $(\sigma_{\max}^2 + \lambda^2)\sigma_{\min}/(\sigma_{\min}^2 + \lambda^2)\sigma_{\max}$ , which is much smaller than its original value  $\sigma_{\max}/\sigma_{\min}$ .

3) Owing to the increasing of the sensitivity and the decreasing of the condition, the convergence probability is higher for the modified Newton algorithm. However, since the step length of  $\Delta\mathbf{x}_m$  declines, the convergence speed is lower compared with the traditional Newton algorithm.

4) A trade-off between the convergence probability and the convergence speed is achieved by changing the singular value factor  $\lambda$ . A larger  $\lambda$  corresponds to a lower convergence probability and a higher convergence speed. In real scene, we usually choose the median of the singular value  $\sigma_i$  as the singular value factor  $\lambda$  for a moderate convergence probability and a moderate convergence speed.

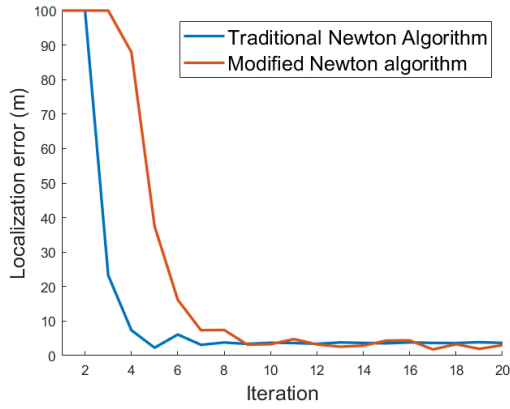
Here, an example is presented to further illustrate the difference between traditional Newton algorithm and the modified Newton algorithm. The geometrical configuration and the noise parameters are the same with Table 1. In case 1, the initial value of the target has a 400 m distance from its real value. In this case, both the traditional Newton algorithm and the modified Newton algorithm have a convergence solution. The localization error for each iteration is given in Figure 4(a), from which, the convergence speed of the modified Newton algorithm is slightly lower than the traditional Newton algorithm, which coincides with the theoretical analysis. In case 2, the initial value of the target has a 1000 m distance from its real value. In this case, the modified Newton algorithm has a convergence solution while the traditional Newton algorithm is non-convergence as shown in Figure 4(b). The traditional Newton algorithm suffers from a large localization error due to the nonconvergence solution, while the proposed modified Newton algorithm remains a high localization precision owing to its convergence solution. To further verify the improvement of the convergence probability, a Monte-Carlo test with 1000 running (for each distance between the initial value and the real value) is implemented, and the result is shown in Figure 5. It is obvious that the modified Newton algorithm has a higher convergence probability than the traditional Newton algorithm when using the improper initial value (distance of the initial value ranges from 300 m to 700 m in the given simulation environment).

### V. LOCALIZATION NODE SELECTION

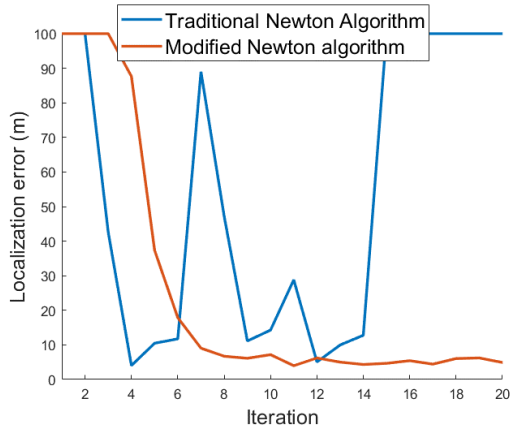
In real situation, the sensors' array is usually fixed on a ship, which travels around the periodic transmitter as shown in Figure 6. Since the ship is moving, the sensors' array receives the periodic signals at different positions (regarded as the localization nodes) and a large amount of localization nodes can be obtained during the whole trajectory. However, considering the computational burden, we cannot use all of the available nodes to achieve the localization. In this case, a localization node selection method is proposed in this section to reduce the computational burden and increase the localization precision.

Firstly, from the localization precision analysis, the localization precision is closely related to the position of the selected localization nodes. Secondly, for real time

$$\mathbf{f}'(\mathbf{x}_m) = \frac{\partial \mathbf{f}}{\partial \mathbf{x}_m} = \begin{bmatrix} \frac{\mathbf{v}_1}{\|\mathbf{c}_1 - \mathbf{x}_m\|_2 \|\mathbf{v}_1\|_2} - \frac{(\mathbf{x}_m - \mathbf{c}_1) \cdot \mathbf{v}_1 \cdot (\mathbf{x}_m - \mathbf{c}_1)}{\|\mathbf{c}_1 - \mathbf{x}_m\|_2^3 \|\mathbf{v}_1\|_2} \cos \alpha_1 \\ \frac{\mathbf{v}_2}{\|\mathbf{c}_2 - \mathbf{x}_m\|_2 \|\mathbf{v}_2\|_2} - \frac{(\mathbf{x}_m - \mathbf{c}_2) \cdot \mathbf{v}_2 \cdot (\mathbf{x}_m - \mathbf{c}_2)}{\|\mathbf{c}_2 - \mathbf{x}_m\|_2^3 \|\mathbf{v}_2\|_2} \cos \alpha_2 \\ \vdots \\ \frac{\mathbf{v}_N}{\|\mathbf{c}_N - \mathbf{x}_m\|_2 \|\mathbf{v}_N\|_2} - \frac{(\mathbf{x}_m - \mathbf{c}_N) \cdot \mathbf{v}_N \cdot (\mathbf{x}_m - \mathbf{c}_N)}{\|\mathbf{c}_N - \mathbf{x}_m\|_2^3 \|\mathbf{v}_N\|_2} \cos \alpha_N \end{bmatrix}$$



(a) Case 1.



(b) Case 2.

FIGURE 4. The localization error for each iteration.

processing, the number of the selected localization nodes is limited (to reduce the computational burden). Thirdly, some localization nodes are with large measurement noise due to the interference or the shielding effect. Considering these facts, the proposed localization node selection method is given as the follow steps.

**Step 1: Rough localization.** Set the number of the localization nodes as 3 and select the localization nodes uniformly during the whole trajectory. Use the modified Newton algorithm to solve the rough location of the target. The rough localization result is used as the initial value for the following localization precision analysis and the accurate localization process.

**Step 2: Localization node selection.** Increase the number of the nodes by 1 and select the initial localization nodes uniformly during the whole trajectory. Then, update the localization nodes as the following step.

- a) Fix node  $c_1, c_2, \dots, c_{N-1}$  and change  $c_N$  ( $N$  is the number of the nodes). Calculate the variation of the theoretical localization precision with  $c_N$  according to (4) and (5) and find the  $\hat{c}_N$  with the optimized localization precision as:

$$\hat{c}_N = \arg \min_{\hat{c}_N=c_N} HDOP(c_1, c_2, \dots, c_N) \quad (18)$$

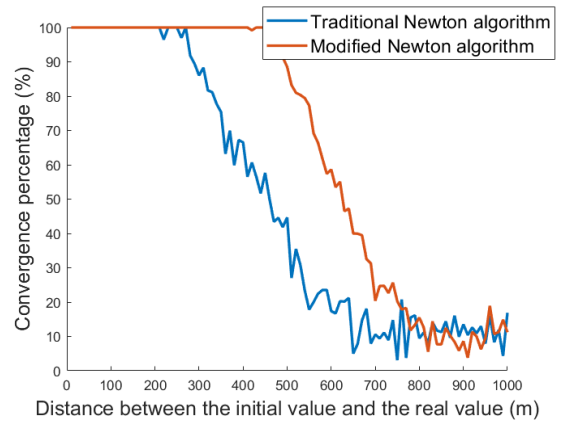


FIGURE 5. The convergence percentage for the traditional Newton algorithm and the modified Newton algorithm.

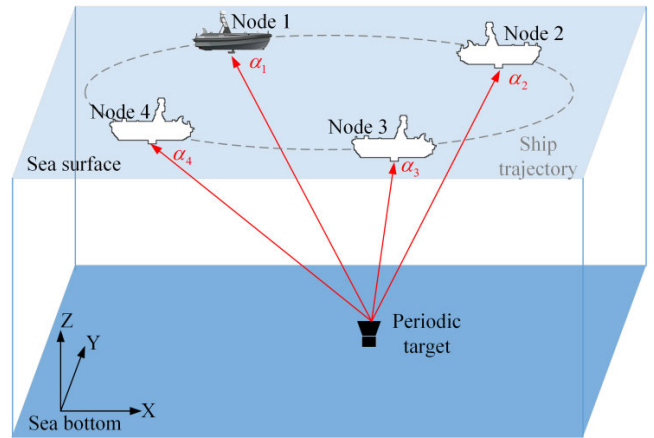


FIGURE 6. Geometrical configuration for the periodic source localization utilizing the ship.

- b) Similar to Step 2a, fix the other nodes ( $c_1, c_2, \dots, c_{n-1}, c_{n+1}, \dots, c_{N-1}$ ) and update each node  $c_n \in [c_1, c_2, \dots, c_{N-1}]$  with the local minimum HDOP as:

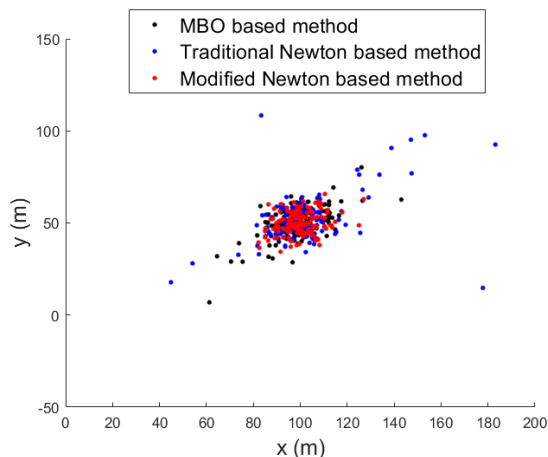
$$\hat{c}_n = \arg \min_{\hat{c}_n=c_n} HDOP(c_1, c_2, \dots, c_n, \dots, c_N) \quad (19)$$

- c) Iterate Step 2a to Step 2b. Once the HDOP reaches its global minimum value, stop the iteration, and the nodes are ascertained for the given node number  $N$ .

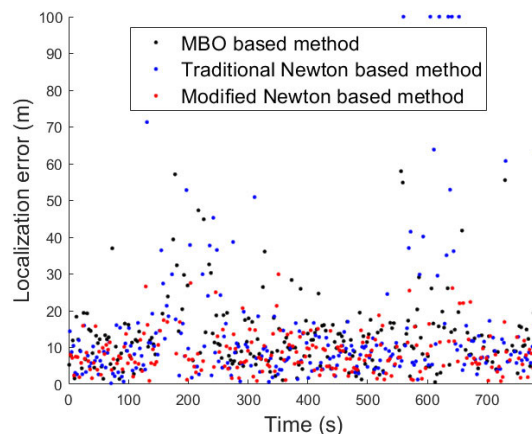
**Step 3: Accurate localization.** Use the modified Newton algorithm to solve the accurate location of the target based on the selected nodes  $c_1, c_2, \dots, c_N$ . Record the localization result as  $\mathbf{x}^{(N)}$  and the value of the cost function  $\mathbf{f}(\mathbf{x}^{(N)})^T \mathbf{Q}_n^{-1} \mathbf{f}(\mathbf{x}^{(N)})$ . If the value of the cost function is lower than the last iteration ( $\mathbf{f}(\mathbf{x}^{(N)})^T \mathbf{Q}_n^{-1} \mathbf{f}(\mathbf{x}^{(N)}) < \mathbf{f}(\mathbf{x}^{(N-1)})^T \mathbf{Q}_n^{-1} \mathbf{f}(\mathbf{x}^{(N-1)})$ ), go to Step 2. Otherwise, stop the iteration and the final localization result is obtained as  $\mathbf{x}^{(N-1)}$ .

## VI. EXPERIMENT

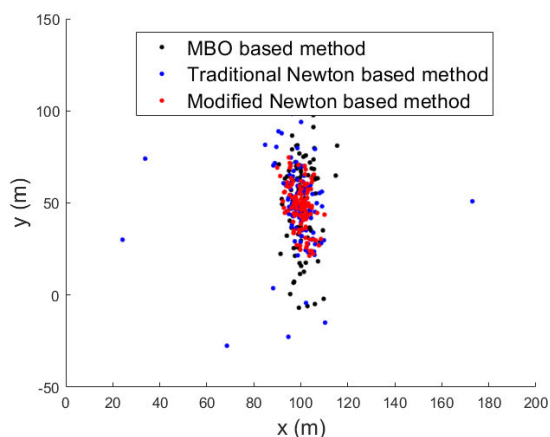
In this section, experiments including the simulation and the lake trial are presented to verify the performance of the



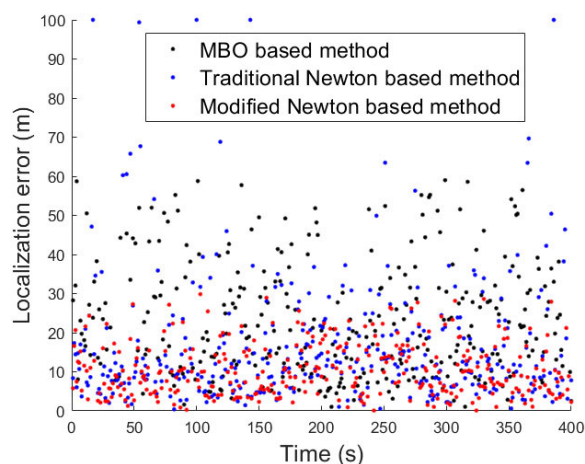
(a) Localization result for the circular path.



(b) Localization error for the circular path.



(c) Localization result for the linear path.



(d) Localization result for the linear path.

FIGURE 7. Localization result and localization error for the simulation.

proposed localization method. The monarch butterfly optimization (MBO) is used as the comparison algorithm owing to its low realization complexity and wide application in localization [25]. Together with the traditional Newton based method and the proposed modified Newton based method, the three methods are utilized to achieve the localization. The geometrical configuration of the simulation and the lake trial is as shown in Figure 6.

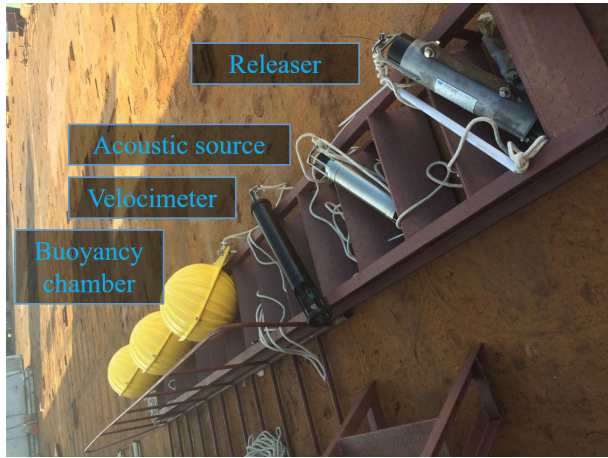
### A. SIMULATION

Circular path and the linear path are two typical trajectories for UWAL. Generally speaking, the circular path has a higher localization precision, but the length of the path is longer. While the linear path is with a lower localization precision and a shorter length. Therefore, the simulation is implemented in two cases. In case 1, the simulated ship travels along a circular path with the speed 2.8 m/s. The center of the circle is [0 0 0] m, and the radius of the circle is 500 m.

In case 2, the simulated ship travels along a linear path from [−1000 500 0] m to [1000 0 0] m with the speed 2 m/s. The simulated receiver is a 4-cell-square-array. The simulated target transmits the periodic signal (signal period 1 s) and the coordinate of the target is  $\mathbf{x} = [100\ 50\ -300]$  m.

The noise environment is the same for the two cases as follows. RMSE of the angular measurement noise ranges from 0.4 degree (300 m) to 0.6 degree (1200 m) according to the distance between the target and the receiver. RMSE of the node’s position measurement noise is 1.8 m. The initial value is randomly distributed around the real value with the RMSE 500 m. The localization result and the variation of the localization error (horizontal error) are shown in Figure 7. The RMSE of the localization result, the convergence probability, and the computational time are given in Table 2.

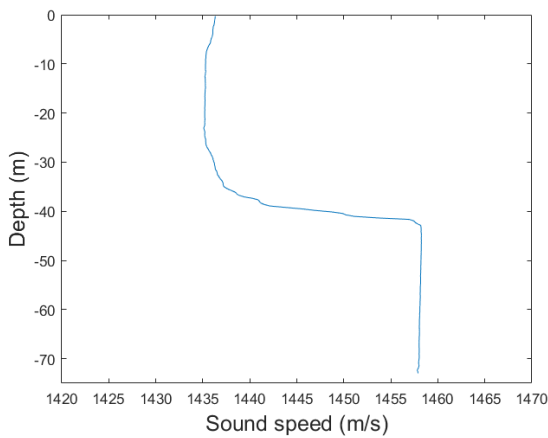
The result indicates that the traditional Newton based method suffers from the nonconvergence problem. The MBO based method and the modified Newton based method



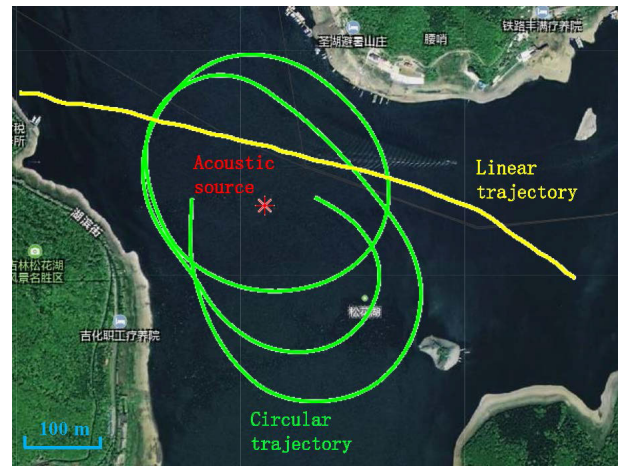
(a) Acoustic source.



(b) USBL sensors' array.



(c) Profile of the sound speed.



(d) Trajectory of the lake trial.

FIGURE 8. The equipment and the environment for the lake trial.

TABLE 2. Performance of the simulation.

	RMSE of the localization result	Convergence percentage	Computational time
Traditional Newton based method for the circular path	21.4 m	97.7	0.06 s
Modified Newton based method for the circular path	12.8 m	100	0.23 s
MBO based method for the circular path	14.4 m	100	0.52 s
Traditional Newton based method for the linear path	36.2 m	95.3	0.06 s
Modified Newton based method for the linear path	16.4 m	100	0.24 s
MBO based method for the linear path	19.9 m	100	0.59 s

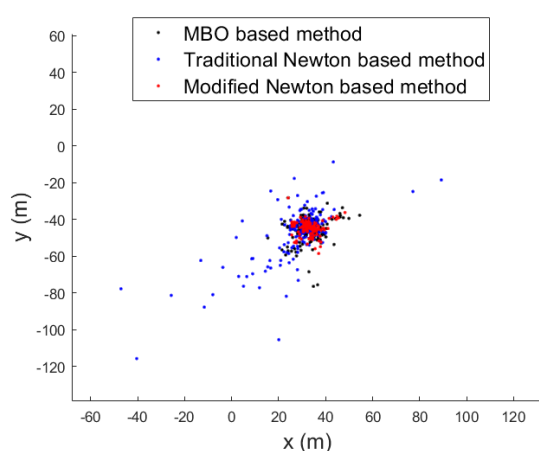
address the problem, and hence, the localization precision is dramatically improved. Compared with the MBO based

method, the modified Newton based method has a higher localization precision due to the carefully selected localization nodes (described in Section V). For the computational time, since we have limited the number of the localization nodes, all of the three compared methods satisfy the real-time process, although, the traditional Newton based method has a lower computational time than the proposed method.

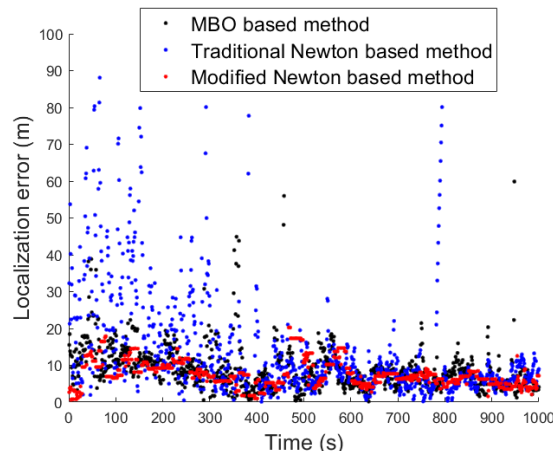
**B. LAKE TRIAL**

To further evaluate the proposed localization method, a lake trial is implemented in Songhua Lake, Jilin Province, China. A periodic acoustic source, shown in Figure 8a, is fixed on the bottom of the lake. The source’s frequency is 40 kHz and the signal period is 1.6 s. The USBL sensors’ array is fixed on the ship at the surface of the sea as shown in Figure 8b. The depth of the source is measured by the velocimeter as 73 m, and the profile of the sound speed is given in Figure 8c. Therefore, the acoustic signal channel is benefit for detecting the direct signal transmitted from the bottom to the surface.

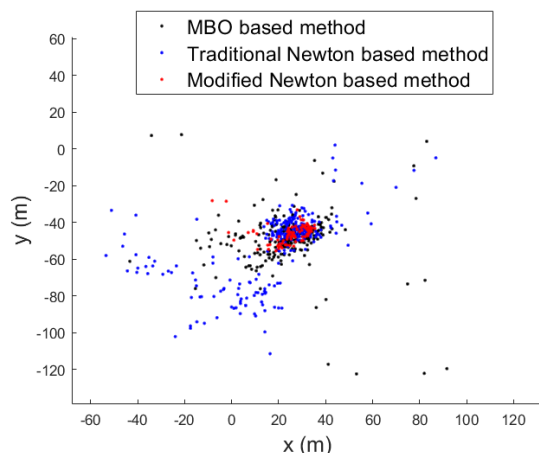




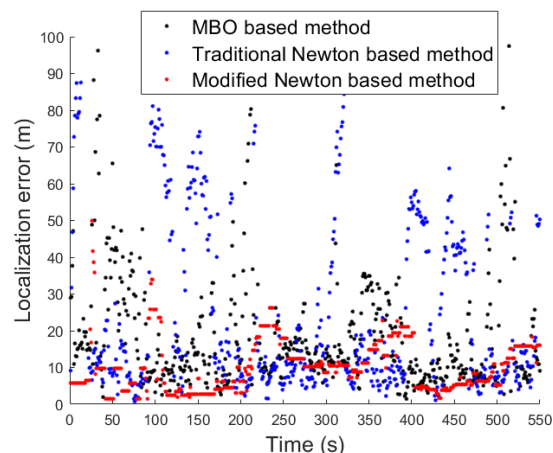
(a) Localization result for the circular path.



(b) Localization error for the circular path.



(c) Localization result for the linear path.



(d) Localization error for the linear path.

FIGURE 9. Localization result and localization error for the lake trial.

The horizontal coordinate of the source is measured by the traditional long base-line UWAL system as [32, -39] m. The ship travels around the source along a certain trajectory (including a circular path and a linear path), and the instantaneous coordinate of the ship is given by the GPS as shown in Figure 8d. We use the MBO based method, the traditional Newton based method, and the modified Newton based method to locate the target. The localization results are given in Table 3 and Figure 9.

The result of the lake trail is similar with the simulation. The modified Newton based method results the highest convergence percentage and the localization precision among the three tested methods. Compared with the simulation result, the lake trial result has a higher localization precision owing to a shorter distance between the target and the trajectory. Compared with the linear path, the circular path has a better performance. It is mainly because that the circular path has a more favorable distribution of the localization nodes, which indicates the necessity of the localization node selection in Section V. The simulation result and the lake trail result prove

TABLE 3. Performance of the lake trial.

	RMSE of the localization result	Convergence percentage	Computational time
Traditional Newton based method for the circular path	16.0 m	96.7	0.08 s
Modified Newton based method for the circular path	7.6 m	100	0.29 s
MBO based method for the circular path	9.7 m	100	0.51 s
Traditional Newton based method for the linear path	26.9 m	92.6	0.08 s
Modified Newton based method for the linear path	12.2 m	100	0.25 s
MBO based method for the linear path	18.8 m	97.6	0.61 s

the effectiveness of the modified Newton based 3-D UWAL method.

**VII. CONCLUSION**

This paper proposes a modified Newton based UWAL method. Compared with the traditional Newton based method and the MBO based method, the proposed method has a higher localization precision and a temperate computational burden. The benefit mainly comes from two aspects. Firstly, a modified Newton algorithm is proposed by introducing the singular value factor, which corrects the ill-condition partial derivative matrix and significantly increases the convergence probability. Secondly, a localization node selection algorithm is presented to achieve the localization node placement. The algorithm optimizes the localization precision and satisfies the real-time process requirement. The simulation and the lake trial are implemented. The results coincide with the theoretical analysis and prove the validity of the proposed method. Our future work will concentrate on applying the method in real application, such as the passive localization of the sailing ship or autonomous underwater vehicle (AUV).

**APPENDIX: DETAILED EXPRESSION OF THE COVARIANCE MATRICES AND THE PARTIAL DERIVATIVE MATRICES**

$$\mathbf{D}_x = \mathbf{M}_x^{-1} \cdot (\mathbf{M}_\alpha \cdot \mathbf{D}_\alpha \cdot \mathbf{M}_\alpha^T + \mathbf{M}_{c1} \cdot \mathbf{D}_{c1} \cdot \mathbf{M}_{c1}^T + \mathbf{M}_{c2} \cdot \mathbf{D}_{c2} \cdot \mathbf{M}_{c2}^T + \dots + \mathbf{M}_{cN} \cdot \mathbf{D}_{cN} \cdot \mathbf{M}_{cN}^T) \cdot \mathbf{M}_x^{-1T}$$

Detailed expressions of the covariance matrices in (4) are as follows.

$$\begin{aligned} \mathbf{D}_x &= \mathbf{E}(\mathbf{e}_x^T \mathbf{e}_x) \\ \mathbf{e}_x &= [e_x \quad e_y \quad e_z] \\ \mathbf{D}_\alpha &= \mathbf{E}(\mathbf{e}_\alpha^T \mathbf{e}_\alpha) = \text{diag}(\sigma_{\alpha 1}^2 \quad \sigma_{\alpha 2}^2 \quad \dots \quad \sigma_{\alpha N}^2) \\ \mathbf{e}_\alpha &= [e_{\alpha 1} \quad e_{\alpha 2} \quad \dots \quad e_{\alpha N}] \\ \mathbf{D}_{c_n} &= \mathbf{E}(\mathbf{e}_{c_n}^T \mathbf{e}_{c_n}) = \text{diag}(\sigma_{a_n}^2 \quad \sigma_{b_n}^2 \quad \sigma_{c_n}^2) \\ \mathbf{e}_{c_n} &= [\sigma_{a_n}^2 \quad \sigma_{b_n}^2 \quad \sigma_{c_n}^2] \end{aligned}$$

where, E() indicates the expectation calculator.  $e_x$ ,  $e_y$ , and  $e_z$  are the localization errors for  $x$  coordinate  $y$  coordinate and  $z$  coordinate, respectively.  $e_{\alpha 1} \quad e_{\alpha 2} \quad \dots \quad e_{\alpha N}$  are the angular measurement errors, and  $\sigma_{\alpha 1}^2 \quad \sigma_{\alpha 2}^2 \quad \dots \quad \sigma_{\alpha N}^2$  are the corresponding mean square errors.  $e_{x_n} \quad e_{y_n} \quad e_{z_n}$  are the node's coordinate measurement errors, and  $\sigma_{a_n}^2 \quad \sigma_{b_n}^2 \quad \sigma_{c_n}^2$  are the corresponding mean square errors.

Detailed expressions of the partial derivative matrices in (4) are as follows.

$$\begin{aligned} \mathbf{M}_x &= \frac{\partial \mathbf{f}}{\partial \mathbf{x}} \\ &= \begin{bmatrix} \frac{\mathbf{v}_1}{\|\mathbf{c}_1 - \mathbf{x}\|_2 \|\mathbf{v}_1\|_2} - \frac{(\mathbf{x} - \mathbf{c}_1) \cdot \mathbf{v}_1 \cdot (\mathbf{x} - \mathbf{c}_1)}{\|\mathbf{c}_1 - \mathbf{x}\|_2^3 \|\mathbf{v}_1\|_2} \cos \alpha_1 \\ \frac{\mathbf{v}_2}{\|\mathbf{c}_2 - \mathbf{x}\|_2 \|\mathbf{v}_2\|_2} - \frac{(\mathbf{x} - \mathbf{c}_2) \cdot \mathbf{v}_2 \cdot (\mathbf{x} - \mathbf{c}_2)}{\|\mathbf{c}_2 - \mathbf{x}\|_2^3 \|\mathbf{v}_2\|_2} \cos \alpha_2 \\ \vdots \\ \frac{\mathbf{v}_N}{\|\mathbf{c}_N - \mathbf{x}\|_2 \|\mathbf{v}_N\|_2} - \frac{(\mathbf{x} - \mathbf{c}_N) \cdot \mathbf{v}_N \cdot (\mathbf{x} - \mathbf{c}_N)}{\|\mathbf{c}_N - \mathbf{x}\|_2^3 \|\mathbf{v}_N\|_2} \cos \alpha_N \end{bmatrix} \\ \mathbf{M}_\alpha &= \frac{\partial \mathbf{f}}{\partial \alpha} = \text{diag}(\sin \alpha_1 \quad \sin \alpha_2 \quad \dots \quad \sin \alpha_N) \end{aligned}$$

$$\begin{aligned} \alpha &= [\alpha_1 \quad \alpha_2 \quad \dots \quad \alpha_N] \\ \mathbf{M}_{c_n} &= \frac{\partial \mathbf{f}}{\partial \mathbf{c}_n} \\ &= \begin{bmatrix} \vdots \\ \frac{\mathbf{v}_n}{\|\mathbf{c}_n - \mathbf{x}\|_2 \|\mathbf{v}_2\|_2} - \frac{(\mathbf{x} - \mathbf{c}_n) \cdot \mathbf{v}_2 \cdot (\mathbf{c}_n - \mathbf{x})}{\|\mathbf{c}_n - \mathbf{x}\|_2^3 \|\mathbf{v}_n\|_2} \cos \alpha_n \\ \vdots \end{bmatrix} \end{aligned}$$

**REFERENCES**

- [1] A. Tariq, F. Azam, M. W. Anwar, T. Zahoor, and A. W. Muzaffar, "Recent trends in underwater wireless sensor networks (UWSNs)—A systematic literature review," *Program. Comput. Softw.*, vol. 46, no. 8, pp. 699–711, Dec. 2020.
- [2] H. Khan, S. A. Hassan, and H. Jung, "On underwater wireless sensor networks routing protocols: A review," *IEEE Sensors J.*, vol. 20, no. 18, pp. 10371–10386, Sep. 2020.
- [3] M. Irshad, W. Liu, L. Wang, and M. U. R. Khalil, "Cogent machine learning algorithm for indoor and underwater localization using visible light spectrum," *Wireless Pers. Commun.*, vol. 116, no. 2, pp. 993–1008, Jan. 2021.
- [4] J. Wang, C. Jiang, H. Zhang, Y. Ren, K.-C. Chen, and L. Hanzo, "Thirty years of machine learning: The road to Pareto-optimal wireless networks," *IEEE Commun. Surveys Tuts.*, vol. 22, no. 3, pp. 1472–1515, 3rd Quart., 2020.
- [5] L. Paull, S. Saeedi, M. Seto, and H. Li, "AUV navigation and localization: A review," *IEEE J. Ocean. Eng.*, vol. 39, no. 1, pp. 131–149, Jan. 2014.
- [6] L. Zhang, C. Tang, P. Chen, and Y. Zhang, "Gaussian parameterized information aided distributed cooperative underwater positioning algorithm," *IEEE Access*, vol. 8, pp. 64634–64645, 2020.
- [7] S. Sun, Y. Chen, L. Qiu, G. Zhang, and C. Zhao, "Inverse synthetic aperture sonar imaging of underwater vehicles utilizing 3-D rotations," *IEEE J. Ocean. Eng.*, vol. 45, no. 2, pp. 563–576, Apr. 2020.
- [8] Y. Wang and Y. Lin, "ISAR imaging of non-uniformly rotating target via range-instantaneous-Doppler-derivatives algorithm," *IEEE J. Sel. Topics Appl. Earth Observ. Remote Sens.*, vol. 7, no. 1, pp. 167–176, Jan. 2014.
- [9] B. Zhang, H. Wang, L. Zheng, J. Wu, and Z. Zhuang, "Joint synchronization and localization for underwater sensor networks considering stratification effect," *IEEE Access*, vol. 5, pp. 26932–26943, 2017.
- [10] M. Jamalabdollahi and S. Zekavat, "ToA ranging and layer thickness computation in nonhomogeneous media," *IEEE Trans. Geosci. Remote Sens.*, vol. 55, no. 2, pp. 742–752, Feb. 2017.
- [11] Z. Li, S. E. Dosso, and D. Sun, "Motion-compensated acoustic localization for underwater vehicles," *IEEE J. Ocean. Eng.*, vol. 41, no. 4, pp. 840–851, Oct. 2016.
- [12] D. J. M. Thomson, S. E. Dosso, and D. R. Barclay, "Modeling AUV localization error in a long baseline acoustic positioning system," *IEEE J. Ocean. Eng.*, vol. 43, no. 4, pp. 955–968, Oct. 2018.
- [13] S. Sun, S. Yu, Z. Shi, J. Fu, and C. Zhao, "A novel single-beacon navigation method for group AUVs based on SIMO model," *IEEE Access*, vol. 6, pp. 75155–75168, 2018.
- [14] S. Sun, X. Zhang, C. Zheng, J. Fu, and C. Zhao, "Underwater acoustical localization of the black box utilizing single autonomous underwater vehicle based on the second-order time difference of arrival," *IEEE J. Ocean. Eng.*, vol. 45, no. 4, pp. 1268–1279, Oct. 2020.
- [15] S. Sun, S. Qin, Y. Hao, G. Zhang, and C. Zhao, "Underwater acoustic localization of the black box based on generalized second-order time difference of arrival (GSTDOA)," *IEEE Trans. Geosci. Remote Sens.*, early access, Nov. 3, 2020, doi: 10.1109/TGRS.2020.3032982.
- [16] F. Ma, C. Xu, X. Zhang, J. He, and W. Su, "Iterative reweighted DOA estimation for impulsive noise processing based on off-grid variational Bayesian learning," *IEEE Access*, vol. 7, pp. 104642–104654, 2019.
- [17] R. Zheng, X. Xu, Z. Ye, and J. Dai, "Robust sparse Bayesian learning for DOA estimation in impulsive noise environments," *Signal Process.*, vol. 171, Jun. 2020, Art. no. 107500.
- [18] V. Varanasi, A. Agarwal, and R. M. Hegde, "Near-field acoustic source localization using spherical harmonic features," *IEEE/ACM Trans. Audio, Speech, Language Process.*, vol. 27, no. 12, pp. 2054–2066, Dec. 2019.

[19] B. T. Hefner and B. R. Dzikowicz, "A spiral wave front beacon for underwater navigation: Basic concept and modeling," *J. Acoust. Soc. Amer.*, vol. 129, no. 6, pp. 3630–3639, Jun. 2011.

[20] B. R. Dzikowicz and B. T. Hefner, "A spiral wave front beacon for underwater navigation: Transducer prototypes and testing," *J. Acoust. Soc. Amer.*, vol. 131, no. 5, pp. 3748–3754, May 2012.

[21] J. Li, Q.-H. Lin, C.-Y. Kang, K. Wang, and X.-T. Yang, "DOA estimation for underwater wideband weak targets based on coherent signal subspace and compressed sensing," *Sensors*, vol. 18, no. 3, p. 902, Mar. 2018.

[22] J. Li, Q.-H. Lin, K. Wang, and C.-Y. Kang, "Performance analysis for focused beamformers in passive underwater acoustic localization," *IEEE Access*, vol. 6, pp. 18200–18208, 2018.

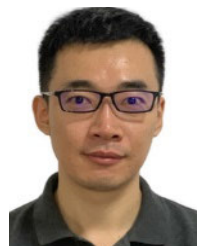
[23] M. Penhale and A. Barnard, "Direction of arrival estimation in practical scenarios using moving standard deviation processing for localization and tracking with acoustic vector sensors," *Appl. Acoust.*, vol. 168, Nov. 2020, Art. no. 107421.

[24] C. E. Zheng, Z. Li, and D. J. Sun, "Study on the calibration method of USBL system based on ray tracing," in *Proc. MTS/IEEE Oceans Conf.*, San Diego, CA, USA, Sep. 2013, pp. 1–4.

[25] I. Strumberger, E. Tuba, N. Bacanin, M. Beko, and M. Tuba, "Monarch butterfly optimization algorithm for localization in wireless sensor networks," in *Proc. 28th Int. Conf. Radioelektronika (RADIOELEKTRONIKA)*, Prague, Czech Republic, Apr. 2018, pp. 1–4.



**LONG QU** received the B.E. and M.E. degrees from Harbin Engineering University, in 2010 and 2013, respectively. He is currently a Senior Engineer with the 703 Research Institute, China State Shipbuilding Corporation Ltd. His research interest includes sonar hardware design.



**YI LOU** received the B.S. degree in communication engineering from Jilin University, in 2009, and the M.S. and Ph.D. degrees in information and communication engineering from the Harbin Institute of Technology, in 2013 and 2017, respectively. He was a Visiting Student with The University of British Columbia, Kelowna, Canada, in 2016. He is currently an Associate Professor with the College of Underwater Acoustic Engineering, Harbin Engineering University.

His research interests include wireless communication and underwater communication.



**XIANG LI** was born in Harbin, China, in 1979. He received the B.E. and Ph.D. degrees from the College of Underwater Acoustic Engineering, Harbin Engineering University, in 2002 and 2010, respectively. He is currently an Assistant Professor with the College of Underwater Acoustic Engineering, Harbin Engineering University. His research interests include sonar hardware design and sonar signal processing.



**XIN LIU** received the B.E. and Ph.D. degrees from Harbin Engineering University. He is currently an Assistant Professor with the College of Underwater Acoustic Engineering, Harbin Engineering University. His research interest includes underwater acoustic localization.



**SIBO SUN** received the B.E. and Ph.D. degrees from the Harbin Institute of Technology, in 2010 and 2017, respectively. He has been studied with the National University of Singapore, since 2014. He is currently an Associate Professor with Harbin Engineering University. His research interests include radar imaging and sonar imaging and positioning.

...